Phys. Status Solidi A **209,** No. 11, 2135–2141 (2012) / **DOI** 10.1002/pssa.201228327

physica status solidi a
www.pss-a.com
applications and materials science

Natural aging of Mg–Gd and Mg–Tb alloys

Jakub Čížek*, Bohumil Smola, Ivana Stulíková, Petr Hruška, Martin Vlach, Marián Vlček, Oksana Melikhova, and Ivan Procházka

Faculty of Mathematics and Physics, Charles University in Prague, V. Holešovičkách 2, 18000 Prague 8, Czech Republic

Received 23 May 2012, revised 12 July 2012, accepted 19 July 2012
Published online 13 August 2012

Keywords aging, alloys, magnesium, point defects, positron annihilation

* Corresponding author: e-mail jakub.cizek@mff.cuni.cz, Phone: +420 221 912 788, Fax: +420 221 912 567

Substantial natural aging occurring on the time scale of less than 1 month was observed in solution-treated Mg–Gd and Mg–Tb alloys. Solution treatment at 500 and 530 °C for Mg–Gd and Mg–Tb alloys, respectively, leads to dissolution of Gd or Tb in the Mg matrix. By quenching of solution-treated alloys to room temperature a supersaturated solid solution of Gd or Tb in Mg was formed. During subsequent aging at ambient temperature the hardness of quenched alloys increases, most probably, due to agglomeration of dissolved Gd or Tb atoms into small clusters. Positron lifetime spectroscopy combined with coincident Doppler broadening revealed that quenched alloys contain vacancies bound to Gd or Tb atoms. Quenched-in vacancies facilitate clustering of Gd or Tb solutes and disappear from the samples when the clusters are fully developed.

1 Introduction Natural aging occurring due to clustering of solute atoms and vacancies at ambient temperature after quenching material from high annealing temperature is well known and investigated in Al-based alloys [1–4]. Solute clusters formed during natural aging hinder movement of dislocations and cause significant strengthening of the material. Natural aging is important for industrial processing since the peak hardness attainable at elevated temperature is affected by the period for which the material was stored at room temperature [5].

Contrary to Al-based alloys natural aging of Mg-based alloys is not common. The Mg–Zn-based alloys are unique in commercial and novel Mg alloys, according to the author's knowledge, where natural aging was reported [6]. An extremely large incubation period (∼9 weeks) was observed in the hardness response to natural aging in binary Mg-7 wt.% Zn alloy and commercial ZK60 alloy. Natural aging starts after a considerably lower period (∼100 h), if specific minor additions as Ti, Cu, Mn, V, or Ba are made [7].

In this work natural aging was observed in binary Mg-alloys with Gd and Tb, which are the basis for novel industrial hardenable Mg alloys with rare-earth elements [8–10].

2 Experimental

2.1 Sample description Binary Mg–Gd alloys with Gd concentration (in wt.%) of 4.48 (Mg4Gd), 9.24 (Mg9Gd), and 14.58 (Mg15Gd), and Mg–Tb alloy with Tb concentration (in wt.%) of 13.39 (Mg13Tb) were produced by squeeze casting under a protective gas atmosphere (Ar + 1% SF_6). The as-cast Mg–Gd and Mg–Tb alloys were subjected to solution treatment at 500 and 530 °C, respectively, for 6 h finished by quenching into water at room temperature. The solution-treated alloys were subsequently naturally aged at ambient temperature (20 °C).

2.2 Hardness testing The Vickers microhardness (HV) testing was carried out using a STRUERS Duramin 300 hardness tester with a load of 100 g applied for 10 s. Solution-treated samples for HV measurements were polished using polishing cloths and 3 μm diamond suspension. No additional polishing was performed during natural aging.

2.3 Electrical resistometry Electrical resistivity was measured at 77 K by means of the dc four-point method with a dummy specimen in series. The influence of any parasitic thermoelectromotive force was suppressed by current reversal.

2.4 Transmission electron microscopy (TEM)

Studies of the microstructure were undertaken on a JEOL JEM 2000FX electron microscope equipped with a LINK AN 1000 microanalyzer.

2.5 Positron annihilation A $^{22}Na_2CO_3$ positron source with activity of 1 MBq deposited on a 2-μm thick mylar foil was always sealed between two pieces of the studied sample.

A digital positron lifetime spectrometer described in Ref. [11] was employed for positron lifetime spectroscopy (PLS) [12]. The spectrometer exhibits excellent time resolution of 145 ps (full width at half-maximum (FWHM) of the resolution function obtained from fitting of positron lifetime spectrum of a well-annealed reference Mg sample). The FWHM of the resolution function that was fitted as a free parameter in decomposition of positron lifetime spectra of the alloys studied, was always (145 ± 1) ps. At least 10^7 annihilation events were accumulated in each positron lifetime spectrum. The source contribution that comes from positrons annihilated in the $^{22}Na_2CO_3$ spot and the covering mylar foil consists of two weak components with lifetimes of 0.368 and 1.5 ns and relative intensities of 8% and 1% and was determined using a well-annealed reference Mg sample.

Coincidence Doppler broadening (CDB) [13] measurements were carried out using a digital spectrometer [14] equipped with two HPGe detectors. The total statistics accumulated in each two-dimensional CDB spectrum was at least 10^8 positron annihilation events. Both PLS and CDB measurements were performed at room temperature. It takes typically ∼2 days to accumulate a single PLS or CDB spectrum with sufficient statistics.

3 Results and discussion

3.1 Solution treatment As-cast alloys subjected to solution treatment were water quenched at regular time intervals and characterized by electrical resistometry and HV in order to monitor dissolution of Gd and Tb in Mg matrix. The electrical resistivity of Mg15Gd and Mg13Tb alloy plotted in Fig. 1a and b, respectively, shows in both alloys a sharp increase at the beginning of the heat treatment followed by an approach to a saturation value. This happens due to the increase of the temperature-independent resistivity component caused by solute enrichment of the matrix. In both alloys HV decreases with annealing time due to dissolution of secondary phases. The annealing for 6 h at 500 °C (MgGd alloys) and 530 °C (MgTb alloy) resulted in a nearly complete dissolution of all secondary phases present in the as-cast states as also revealed by TEM observations.

3.2 Natural aging Development of HV during natural aging of MgGd alloys and Mg13Tb alloy is shown in Fig. 2a and b, respectively. Obviously HV rises with increasing aging time in both alloys. The time dependence of HV plotted in the logarithmic time scale exhibits an S-shaped curve typical of natural aging.

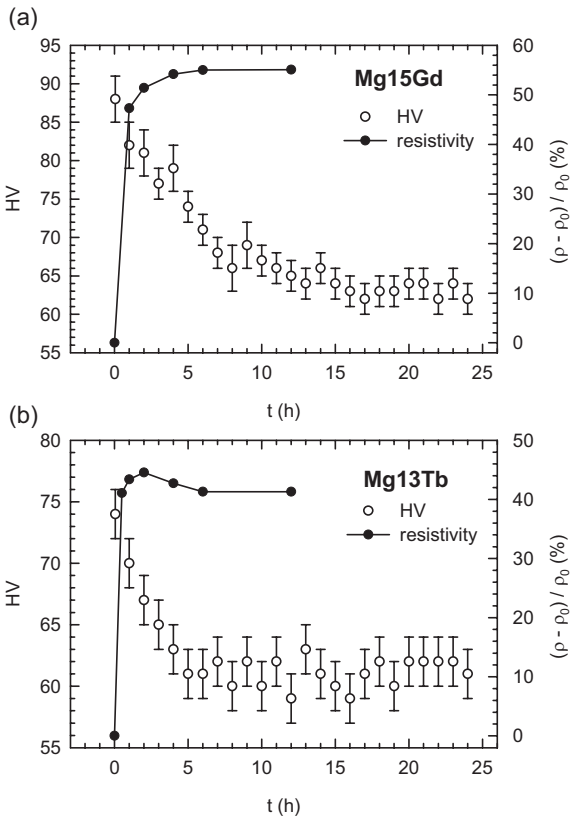

Figure 1 Development of HV and the relative change of electrical resistivity $(\rho - \rho_0)/\rho_0$ during solution treatment. The symbol ρ_0 denotes the electrical resistivity of the as-cast sample while ρ is the electrical resistivity of the sample solution treated for the time t; (a) results for Mg15Gd alloy solution treated at 500 °C; (b) results for Mg13Tb alloy solution treated at 530 °C.

Since the solubility of Gd and Tb in Mg decreases strongly with decreasing temperature a supersaturated solid solution is formed in quenched alloys. Using electron diffraction (ED) in TEM no extra spots (except for those for the Mg matrix) were observed in ED patterns of the Mg13Tb and Mg15Gd alloy specimens naturally aged for 240 h, when the aging is almost finished, see Fig. 2. The first evidence for metastable ordered phase precipitation in these solution-treated alloys was found in the ED pattern after isochronal annealing up to 180 °C in Mg13Tb alloy – Fig. 3 and up to 200 °C in Mg15Gd [15] only. The precipitates in both alloys were identified as very small particles of the ordered hexagonal $D0_{19}$ phase giving diffuse reflection spots. As no development of any transient phase known from decomposition of Mg-rare earth alloys was proved by ED in naturally aged Mg13Tb and Mg15Gd alloys, clustering of solute atoms should be, most probably, regarded as responsible for the natural aging. The driving force for this process is the solute supersaturation in the Mg matrix.

Diffusion of alloying elements (Gd and Tb) necessary for formation of clusters can be facilitated by quenched-in vacancies. To examine this hypothesis we employed two complementary techniques of positron annihilation

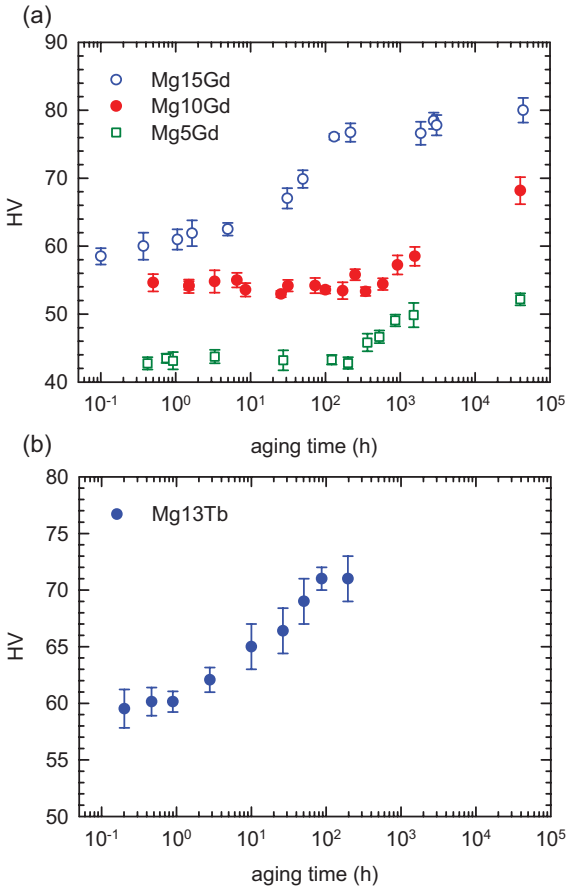

Figure 2 (online color at: www.pss-a.com) Development of hardness in (a) MgGd alloys and (b) Mg13Tb alloy aged at ambient temperature. Each point in the figure was obtained as an average of 10 measurements performed within 10 min.

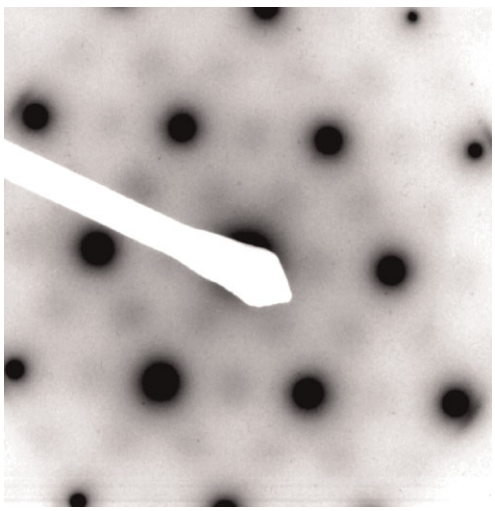

Figure 3 $[0001]_{\alpha\text{-Mg}}$ zone ED pattern of solution-treated Mg13Tb alloy isochronally annealed up to 180 °C. Note the diffuse reflection spots of the ordered hexagonal $D0_{19}$ phase in the middle positions between the α-Mg matrix spots.

spectroscopy: PLS that enables detection of quenched-in vacancies and determines their concentration [12] and CDB that provides the distribution of momentum p of electrons that annihilated positrons and carries information about chemical environment of vacancies [13]. Positron lifetimes and corresponding relative intensities determined by PLS are listed in Table 1. The solution-treated alloys measured immediately after quenching exhibit two-component spectra. The shorter component with lifetime τ_1 comes from free positrons. The lifetime of the second component $\tau_2 \approx 300$ ps is comparable to that of a monovacancy in Mg [16].

Positive correlation between the solute and vacancy binding energy and the solute size is well documented for dilute Al alloys [17, 18]. A large impurity atom placed into the matrix imposes a significant strain on the surrounding atoms. A vacancy located next to this large impurity atom allows the impurity to relax to the open volume in the vacancy. Such inward relaxation of the impurity towards the vacancy releases the strain imposed on the neighboring atoms and causes an energy decrease [17]. However, the solute size effect alone cannot explain very small or even negative vacancy binding energies to 3d transition-metal solutes [17] that are explained by formation of strong bonds between 3d transition metals and Al atoms [18]. In analogy with Al alloys one could expect attractive interaction between vacancies and Gd or Tb solutes having larger size than Mg atoms. However, since both Gd and Tb have an incompletely filled f-shell this can be changed or even reversed due to binding between Gd or Tb solutes and Mg atoms. The vacancy–solute binding energy influences the concentration of vacancies associated with Gd or Tb atoms formed during solution treatment at elevated temperature. Single vacancies in Mg are mobile well bellow room temperature and in quenched samples quickly disappear by diffusion to sinks at the surface and grain boundaries [19]. However, vacancy–Gd (or –Tb) pairs are most probably more stable and may remain in the quenched alloys. Hence, the component with the lifetime τ_2 can be attributed to positrons trapped in vacancies bound to Gd or Tb atoms.

Note that vacancies in Mg are relatively shallow positron traps [20]. This is reflected by intensities I_2 of trapped positrons that are lower compared to those typical for solution-treated Al alloys [3, 4]. The concentration c_{pairs} of quenched-in vacancy–Gd (or –Tb) pairs can be calculated from PLS data using the simple trapping model (STM) [21]

$$c_{\text{pairs}} = \frac{1}{\nu_v} I_2 \left(\frac{1}{\tau_1} - \frac{1}{\tau_2} \right), \tag{1}$$

where $\nu_v = 1.1 \times 10^{13}\ \text{s}^{-1}$ is the specific positron trapping rate for a vacancy in Mg [22].

Figure 4 shows c_{pairs} calculated by Eq. (1) for solution-treated alloys with various concentrations c of the alloying elements (Gd or Tb). Obviously, c_{pairs} increases with increasing solute concentration c. The equilibrium concentration c^*_{pairs} of vacancies associated with Gd or Tb atoms at

Table 1 Results of PLS measurements: lifetimes τ_i and relative intensities I_i of the components resolved in positron lifetime spectra for solution-treated alloys measured immediately after quenching (quenched alloys) and after aging at ambient temperature for at least 2 months (aged alloys). Note that single PLS measurement took ~2 days.

sample	quenched alloys				aged alloys	
	τ_1 (ps)	I_1 (%)	τ_2 (ps)	I_2 (%)	τ_1 (ps)	I_1 (%)
Mg4Gd	219.7 (5)	92.5 (5)	290 (10)	7.5 (5)	225.5 (2)	100
Mg9Gd	218.6 (5)	88.4 (5)	300 (5)	11.6 (5)	225.2 (2)	100
Mg15Gd	214.6 (7)	80.5 (6)	295 (5)	19.5 (6)	225.4 (2)	100
Mg13Tb	214.0 (8)	84.3 (7)	280 (15)	15.7 (7)	225.5 (2)	100

the solution-treatment temperature T is determined by the probability that a lattice site is vacant (given by the equilibrium concentration of vacancies) multiplied by the probability that a next site is occupied by a solute atom (given by the atomic concentration c of Gd or Tb solutes) and a correlation factor that accounts for the effect of solute–vacancy binding energy. Hence, the equilibrium concentration of vacancies associated with Gd or Tb atoms is expressed by the equation [23, 24]

$$c^*_{\text{pairs}} = \exp\left(\frac{S_{\text{v,f}}}{k}\right)\exp\left(-\frac{E_{\text{v,f}}}{kT}\right) c\, Z \exp\left(\frac{E_{\text{b}}}{kT}\right), \qquad (2)$$

where k is the Boltzmann constant, $Z = 12$ is the coordination number in the hexagonal lattice and $S_{\text{v,f}} \approx 2\,k$ [25] is the vacancy formation entropy. The vacancy formation enthalpy $E_{\text{v,f}}$ in Mg was reported by several authors. Janot et al. [26] in their early work obtained a rather low value $E_{\text{v,f}} = 0.58$ eV from the comparison of dilatometric and X-ray lattice expansion measurements at elevated temperatures. This experiment was later criticized by Tzanetakis et al. [19] because the dilatometric and X-ray experiments were not performed on the same specimen. Indeed, electrical resistivity measurements at thermal equilibrium or after quenching yielded considerably larger values $E_{\text{v,f}} = 0.79 \pm 0.03$ [19] and $E_{\text{v,f}} = 0.83 \pm 0.03$ eV [27]. A comparable value $E_{\text{v,f}} \approx 0.85$ eV was obtained employing positron annihilation spectroscopy [28]. Krimmel and Fahnle [29] also obtained a similar value $E_{\text{v,f}} = 0.83 \pm 0.07$ eV using *ab initio* theoretical calculations. Hence, from an analysis of the literature we can conclude that the vacancy formation energy for Mg vacancy falls most probably into the range 0.79–0.85 eV.

The solute–vacancy binding energy E_{b} is not known so far. Putting $E_{\text{b}} \approx 0$ into Eq. (2) gives a bound for c^*_{pairs} corresponding to no binding and no repulsion between vacancies and solute atoms. This estimate of c^*_{pairs} is shown in Fig. 4 by a shaded band between the border lines corresponding to $E_{\text{v,f}} = 0.79$ and 0.85 eV. Obviously, c^*_{pairs} bound estimated by Eq. (2) using $E_{\text{b}} \approx 0$ is slightly lower than the concentration of quenched-in defects c_{pairs} determined by PLS. This suggests a small positive binding energy between Gd (or Tb) solute and vacancy ($E_{\text{b}} < 0.1$ eV). *Ab initio* theoretical calculations performed recently by Huber et al. [30] resulted in a small but negative binding energy between vacancy and Gd solute ($-0.05\,\text{eV} < E_{\text{b}} < 0\,\text{eV}$). Hence, further investigations are necessary to achieve a definite conclusion about binding energy between vacancies and Gd (or Tb) solute.

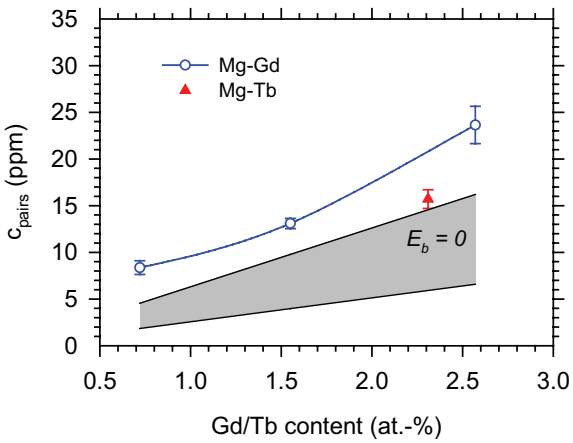

Figure 4 (online color at: www.pss-a.com) The concentration c_{pairs} of quenched-in vacancy–Gd (open circles) and vacancy–Tb (full triangle) pairs determined in solution-treated alloys by PLS. The shaded area shows the band for the equilibrium concentration of vacancy–Gd (or –Tb) pairs at temperature of 500 °C calculated by Eq. (2) under assumption of no binding between vacancies and solutes ($E_{\text{b}} = 0$).

It took ~2 days to accumulate a positron lifetime spectrum with sufficient statistics. During the measurement partial positron lifetime spectra were recorded every hour and analyzed in terms of the mean positron lifetime (center of mass of positron lifetime spectrum with subtracted source contribution and constant background) in order to monitor the stability of solute–vacancy pairs in the sample. No changes of the mean positron lifetime except that of statistical scattering were observed in all alloys studied. This testifies that quenched-in vacancies remain in the sample at least for 2 days. To further characterize the stability of vacancies positron lifetime investigations of solution-treated Mg15Gd alloy were performed for an extended period of 140 h (~6 days). Again no changes of the mean positron lifetime were observed except for statistical scattering. Hence, we can conclude that quenched-in vacancies remain in the naturally aged Mg15Gd alloy at least for 6 days.

On the other hand, the alloys aged at ambient temperature for 2 months or more, also shown in Table 1 exhibit a single-component positron lifetime spectra with lifetime $\tau_1 \approx 225$ ps, which agrees with the bulk positron lifetime in Mg [16]. This testifies that quenched-in vacancies were removed when the solute clusters developed.

CDB results for Mg15Gd alloy measured immediately after quenching and aged at ambient temperature for 2 months are plotted in Fig. 5 as ratio curves (related to well annealed pure Mg). Following the approach developed by Somoza et al. [31] and applied successfully for analysis of CDB data in Al-based [31, 32] and Mg-based alloys [33] the high-momentum part of the momentum distribution $n(p)$ of annihilating electron–positron pairs in the Mg15Gd alloy can be expressed as a superposition of several contributions

$$n = (1-F)\left(\xi_{\mathrm{Mg,f}} n_{\mathrm{Mg,f}} + \xi_{\mathrm{Gd,f}} n_{\mathrm{Gd,f}}\right) + F\left(\xi_{\mathrm{Mg,v}} n_{\mathrm{Mg,v}} + \xi_{\mathrm{Gd,v}} n_{\mathrm{Gd,v}}\right), \quad (3)$$

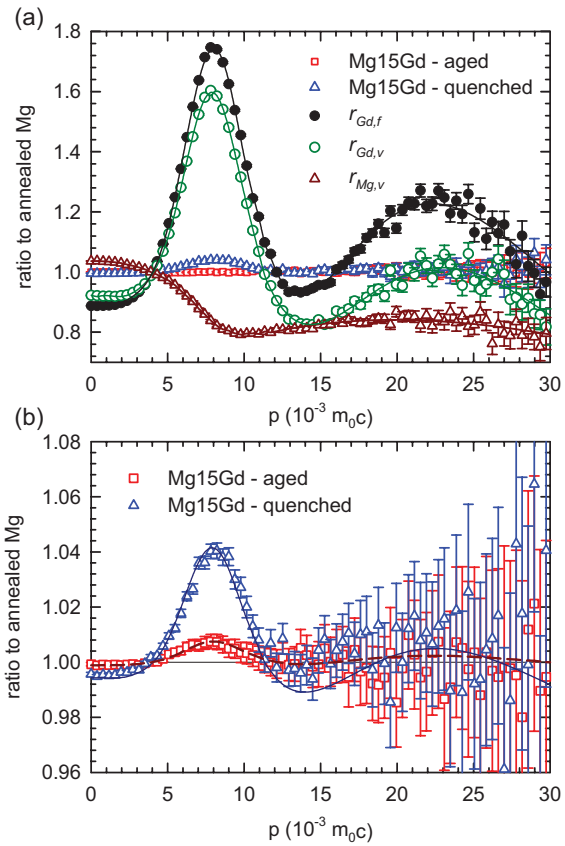

Figure 5 (online color at: www.pss-a.com) (a) CDB ratio curves (related to well-annealed pure Mg) for Mg15Gd alloy measured immediately after quenching (open triangles) and after natural aging for 2 months (open squares). Reference ratio curves $r_{\mathrm{Mg,v}}$, $r_{\mathrm{Gd,f}}$, and $r_{\mathrm{Gd,v}}$ used in Eq. (6) are plotted in the figure as well; (b) detail of the ratio curves for Mg15Gd alloy. Solid and dashed lines show model curve calculated by Eq. (6) for quenched and aged sample, respectively.

where $n_{\mathrm{Mg,f}}$ and $n_{\mathrm{Gd,f}}$ denote the momentum distribution of free positrons annihilated by Mg and Gd electrons, respectively, while the momentum distribution of positrons trapped at vacancies and annihilated by Mg and Gd electrons, respectively, is denoted $n_{\mathrm{Mg,v}}$ and $n_{\mathrm{Gd,v}}$. The weights $\xi_{\mathrm{Mg,f}}$ and $\xi_{\mathrm{Gd,f}}$ represent the fractions of free positrons annihilated by Mg and Gd electrons, respectively, and always satisfy the normalization condition $\xi_{\mathrm{Mg,f}} + \xi_{\mathrm{Gd,f}} = 1$. Similarly $\xi_{\mathrm{Mg,v}}$ and $\xi_{\mathrm{Gd,v}}$ denote the fraction of positrons trapped at vacancies and annihilated by Mg and Gd electrons, respectively. Again these weights satisfy the normalization condition $\xi_{\mathrm{Mg,v}} + \xi_{\mathrm{Gd,v}} = 1$. The symbol F stands for the fraction of positrons trapped at vacancies.

The momentum distributions $n_{\mathrm{Mg,f}}$ and $n_{\mathrm{Mg,v}}$ were obtained using reference samples of pure Mg (99.99%). Well annealed (400 °C/1 h) Mg exhibits a single-component positron lifetime spectrum with lifetime of (225.0 ± 0.5) ps that testifies that virtually all positrons are annihilated in the free state. Hence, the momentum distribution measured in the well-annealed Mg equals $n_{\mathrm{Mg,f}}$. Another pure Mg sample was cold rolled to a thickness reduction of 35%. The cold-rolled sample exhibits a two-component positron lifetime spectrum. The shorter component with lifetime $\tau_1 = (210 \pm 4)$ ps and intensity $I_1 = (60\pm)\%$ comes from free positrons, while the longer component with the lifetime $\tau_2 = (256 \pm 2)$ ps and intensity $I_2 = (40 \pm 2)\%$ represents a contribution of positrons trapped at dislocations introduced by plastic deformation [34]. It is well known that a dislocation line itself is only a shallow positron trap. Once a positron is trapped at a dislocation line it quickly diffuses along it and is finally trapped at a vacancy anchored in the elastic field of the dislocation [35]. Thus, the momentum distributions obtained for positrons trapped at vacancy-like defects in deformed metals can be used as a good approximation of those for positrons trapped at vacancies [31]. The momentum distribution measured in cold-rolled pure Mg can be expressed as

$$n_{\mathrm{CR\text{-}Mg}} = (1-F)\xi_{\mathrm{Mg,f}} n_{\mathrm{Mg,f}} + F\xi_{\mathrm{Mg,v}} n_{\mathrm{Mg,v}}. \quad (4)$$

The fraction F of positrons trapped at defects (here vacancies attached to dislocations) can be calculated from positron lifetime results [12]

$$F = I_2 \frac{\tau_2 - \tau_1}{\tau_2}. \quad (5)$$

Hence, combining Eqs. (4) and (5) the momentum distribution $n_{\mathrm{Mg,v}}$ was determined.

A similar procedure was applied for determination of the momentum distributions $n_{\mathrm{Gd,f}}$ and $n_{\mathrm{Gd,v}}$. A well-annealed (850 °C/1 h) pure Gd (99.9%) sample exhibits a single-component positron lifetime spectrum with lifetime of (205.5 ± 0.5) ps that agrees well with the Gd bulk positron lifetime [16]. Hence, the momentum distribution measured in the well-annealed Gd sample equals to $n_{\mathrm{Gd,f}}$. Another pure Gd sample was cold rolled to thickness reduction of 50%.

The cold-rolled sample exhibits a single-positron spectrum with lifetime of (280 ± 5) ps testifying that virtually all positrons are annihilated from trapped states at vacancy-like defects attached to dislocations. Hence, the momentum distribution measured in the cold-rolled Gd sample can be used as a good approximation for $n_{\mathrm{Gd,v}}$.

To highlight the differences between momentum distributions for various positron states the CDB results in Fig. 5 are presented as ratio curves related to well-annealed Mg, that is, all momentum distributions are divided by $n_{\mathrm{Mg,f}}$. The ratio curve $r = n/n_{\mathrm{Mg,f}}$ for Mg15Gd alloy can be expressed as

$$r = (1-F)(1-\xi_{\mathrm{Gd,f}}+\xi_{\mathrm{Gd,f}}r_{\mathrm{Gd,f}}) + F((1-\xi_{\mathrm{Gd,v}})r_{\mathrm{Mg,v}}+\xi_{\mathrm{Gd,v}}r_{\mathrm{Gd,v}}), \quad (6)$$

where $r_{\mathrm{Gd,f}} = n_{\mathrm{Gd,f}}/n_{\mathrm{Mg,f}}$ is the ratio curve for free positrons annihilated by Gd electrons, $r_{\mathrm{Mg,v}} = n_{\mathrm{Mg,v}}/n_{\mathrm{Mg,f}}$ is the ratio curve for positrons trapped at vacancies and annihilated by Mg electrons, and $r_{\mathrm{Gd,v}} = n_{\mathrm{Gd,v}}/n_{\mathrm{Mg,f}}$ is the ratio curve for positrons trapped at vacancies and annihilated by Gd electrons. The ratio curves $r_{\mathrm{Gd,f}}$, $r_{\mathrm{Mg,v}}$, and $r_{\mathrm{Gd,v}}$ are plotted in Fig. 5a. The ratio curve $r_{\mathrm{Mg,v}}$ is enhanced at low momenta and lowered in the high momentum region since the probability that a positron localized in a vacancy is annihilated by a high-momentum core electron is reduced. The ratio curve $r_{\mathrm{Gd,f}}$ for free positrons annihilated by Gd electrons exhibits a peak at the momentum $p \approx 8 \times 10^{-3}\, m_0 c$ followed by a broader peak at $p \approx 23 \times 10^{-3}\, m_0 c$. The ratio curve $r_{\mathrm{Gd,v}}$ exhibits similar shape as $r_{\mathrm{Gd,f}}$ but is shifted down in the high-momentum range and shifted up at low momenta. This is again due to the effect of positron confinement in a vacancy increasing the probability that positron is annihilated by a low-momentum valence electron and lowering the probability that it is annihilated by a high-momentum core electron.

The fraction $F = (5.3 \pm 0.5)\%$ of positrons trapped at vacancies was calculated from Eq. (5) using positron lifetime results for the quenched Mg15Gd alloy given in Table 1. Since the concentration of vacancies associated with Gd atoms is roughly three orders of magnitude smaller than the concentration of Gd atoms ($c_{\mathrm{pairs}} << c$) most of the dissolved Gd atoms are not associated with vacancies and the probability that a free positron will be by a chance annihilated by a Gd electron is in the first approximation equal to the atomic concentration of Gd atoms, $\xi_{\mathrm{Gd,f}} \approx c = 2.57$ at.%. Hence, the weight $\xi_{\mathrm{Gd,v}}$ is the only remaining unknown parameter in Eq. (6) and it was obtained by fitting of r to the experimental points. The solid line in Fig. 5 shows the ratio curve r calculated by Eq. (6) for the quenched Mg15Gd alloy. The best agreement with experimental points was obtained for $\xi_{\mathrm{Gd,v}} = (75 \pm 5)\%$. Hence, a positron trapped at a vacancy is annihilated by a Gd electron with a high probability. This result testifies that quenched-in vacancies in Mg15Gd alloy are indeed associated with Gd atoms.

The CDB ratio curve for Mg15Gd sample aged for 2 months exhibits a significantly lower contribution of positrons annihilated Gd electrons. Positron lifetime values in Table 1 revealed that virtually all positrons in the aged sample annihilate from the free state, that is, $F \approx 0$ and Eq. (6) takes a particularly simple form without any fitting parameter. The ratio curve r calculated by Eq. (6) for the aged Mg15Gd sample and plotted in Fig. 5 by a dashed line is in satisfactory agreement with the experimental points. Hence, the CDB results support the picture drawn from the PLS investigations that vacancies are removed when the clusters developed. Free positron delocalized in the lattice can still be annihilated by chance by a Gd electron. But the probability that it happens is significantly lower than for a positron trapped at a vacancy associated with a Gd atom.

4 Conclusions In summary, natural aging of Mg–Gd and Mg–Tb alloys was observed in this work. Hardening of these alloys during aging at ambient temperature occurs, most probably, due to agglomeration of dissolved Gd or Tb atoms into small clusters. Diffusion of Gd or Tb atoms is facilitated by quenched-in vacancies that disappear when the formation of clusters is finished.

Acknowledgements This work was supported by the Czech Science Foundation (project P108/10/0648), the Academy of Science of Czech Republic (project KAN300100801), and the Charles University (grant SVV-2012-265303). The work of O.M. is a part of activities of the Charles University Research Center "Physics of Condensed Matter and Functional Materials."

References

[1] S. Esmaeili, D. J. Lloyd, and W. J. Poole, Acta Mater. **51**, 3467 (2003).
[2] I. Stulíková, J. Faltus, and B. Smola, Kovove Mater. **45**, 85 (2007).
[3] B. Klobes, T. E. M. Staab, M. Haaks, K. Maier, and I. Wieler, Phys. Status Solidi RRL **2**, 224 (2008).
[4] J. Banhart, M. D. H. Lay, C. S. T. Chang, and J. Hill, Phys. Rev. B **83**, 014101 (2011).
[5] D. W. Pashley, J. W. Rhodes, and A. Sendorek, J. Inst. Met. **94**, 41 (1966).
[6] J. Buha, J. Mater. Sci. **43**, 1120 (2008).
[7] J. Buha, Acta Mater. **56**, 3533 (2008).
[8] I. A. Anyanwu, Y. Kitaguchi, I. Harima, S. Kamado, Y. Kojima, S. Tanike, and I. Seki, in: Magnesium 97, edited by E. Agion and D. Eliezer (Magnesium Research Inst. (MRI) Ltd., Beer-Sheva, 1997), pp. 127–132.
[9] B. L. Mordike and T. Ebert, Mater. Sci. Eng. A **302**, 37 (2001).
[10] B. L. Mordike, Mater. Sci. Eng. A **324**, 103 (2002).
[11] F. Bečvář J. Čížek, I. Procházka, and J. Janotová, J. Nucl. Instrum. Methods A **539**, 372 (2005).
[12] P. Hautojärvi and C. Corbel, in: Positron spectroscopy of solids, Proc. Int. School of Physics "Enrico Fermi", edited by A. Dupasquier and A. P. Mills (IOS Press, Amsterdam, 1995), p. 491.
[13] P. Asoka-Kumar, M. Alatalo, V. J. Ghosh, A. C. Kruseman, B. Nielsen, and K. G. Lynn, Phys. Rev. Lett. **77**, 2097 (1996).
[14] J. Čížek, M. Vlček, and I. Procházka, Nucl. Instrum. Methods A **623**, 982 (2010).

[15] P. Vostrý, B. Smola, I. Stulíková, F. von Buch, and B. L. Mordike, Phys. Status Solidi A **175**, 491 (1999).
[16] J. M. Campillo Robles, E. Ogando, and F. Plazaola, J. Phys.: Condens. Matter **19**, 176222 (2007).
[17] C. Wolverton, Acta Mater. **55**, 5867 (2007).
[18] M. Ohta and F. Hashimoto, J. Phys. Soc. Jpn. **19**, 1987 (1964).
[19] P. Tzanetakis, J. Hillairet, and G. Revel, Phys. Status Solidi B **75**, 433 (1976).
[20] P. Hautojärvi, J. Johansson, A. Vehanen, J. Yli-Kauppila, J. Hillairet, and P. Tzanétakis, Appl. Phys. A **27**, 49 (1982).
[21] R. West, in: Positrons in Solids, edited by P. Hautojärvi (Springer-Verlag, Berlin, 1979), p. 89.
[22] G. M. Hood, Phys. Rev. B **26**, 1036 (1982).
[23] T. R. Anthony, Acta Metall. **17**, 603 (1969).
[24] M. Doyama, J. Nucl. Mater. **69/70**, 350 (1978).
[25] H. Wollenberger, in: Physical Metallurgy, Vol. 2, eidted by R. Cahn and P. Haasen (North-Holland, Amsterdam, 1983), p. 1146.
[26] C. Janot, D. Malléjac, and B. George, Phys. Rev. B **2**, 3088 (1970).
[27] P. Tzanetakis, Thése, Université des Grenoble 1978.
[28] P. Hautojärvi, J. Johansson, A. Vehanen, and J. Yli-Kauppila, Appl. Phys. A **27**, 49 (1982).
[29] H. Krimmel and M. Fähnle, Phys. Rev. B **62**, 5489 (2000).
[30] L. Huber, I. Elfimov, J. Rottler, and M. Militzer, Phys. Rev. B **85**, 144301 (2012).
[31] A. Somoza, M. P. Petkov, K. G. Lynn, and A. Dupasquier, Phys. Rev. B **65**, 094107 (2002).
[32] A. Somoza and A. Dupasquier, J. Mater. Process. Technol. **135**, 83 (2003).
[33] P. Mengucci, G. Barucca, G. Riontino, D. Lussana, M. Massazza, R. Ferragut, and E. Hassan Aly, Mater. Sci. Eng. A **479**, 37 (2008).
[34] J. Čížek, I. Procházka, B. Smola, I. Stulíková, and V. Očenášek, J. Alloys Compd. **430**, 92 (2007).
[35] L. C. Smedskjaer, M. Manninen, and M. J. Fluss, J. Phys. F **10**, 2237 (1980).